Journal of Astronomical Telescopes, Instruments, and Systems

AstronomicalTelescopes.SPIEDigitalLibrary.org

Baseline requirements for detecting biosignatures with the HabEx and LUVOIR mission concepts

Ji Wang
Dimitri Mawet
Renyu Hu
Garreth Ruane
Jacques-Robert Delorme
Nikita Klimovich

SPIE.

Ji Wang, Dimitri Mawet, Renyu Hu, Garreth Ruane, Jacques-Robert Delorme, Nikita Klimovich, "Baseline requirements for detecting biosignatures with the HabEx and LUVOIR mission concepts," *J. Astron. Telesc. Instrum. Syst.* **4**(3), 035001 (2018), doi: 10.1117/1.JATIS.4.3.035001.

Baseline requirements for detecting biosignatures with the HabEx and LUVOIR mission concepts

Ji Wang,[a,*] Dimitri Mawet,[a] Renyu Hu,[b,c] Garreth Ruane,[a] Jacques-Robert Delorme,[a] and Nikita Klimovich[a]
[a]California Institute of Technology, Department of Astronomy, Pasadena, California, United States
[b]California Institute of Technology, Jet Propulsion Laboratory, Pasadena, California, United States
[c]California Institute of Technology, Division of Geological and Planetary Sciences, Pasadena, California, United States

Abstract. A milestone in understanding life in the universe is the detection of biosignature gases in the atmospheres of habitable exoplanets. Future mission concepts under study by the 2020 decadal survey, e.g., Habitable Exoplanet Imaging Mission (HabEx) and the Large UV/Optical/IR Surveyor (LUVOIR), have the potential of achieving this goal. We investigate the baseline requirements for detecting four molecular species, H_2O, O_2, CH_4, and CO_2, assuming concentrations of these species equal to that of modern Earth. These molecules are highly relevant to habitability and life on Earth and other planets. Through numerical simulations, we find the minimum requirements of spectral resolution, starlight suppression, and exposure time for detecting biosignature and habitability marker gases. The results are highly dependent on cloud conditions. A low-cloud case is more favorable because of deeper and denser lines whereas a no-cloud case is the pessimistic case for its low albedo. The minimum exposure time for detecting a certain molecule species can vary by a large factor (∼10) between the low-cloud case and the no-cloud case. For all cases, we provide baseline requirements for HabEx and LUVOIR. The impact of exozodiacal contamination and thermal background is also discussed and will be included in future studies. [DOI: 10.1117/1.JATIS.4.3.035001]

Keywords: Habitable Exoplanet Imaging Mission; Large UV/Optical/IR Surveyor; biosignature; life; high dispersion coronagraphy.
Paper 17071P received Aug. 30, 2017; accepted for publication Jun. 6, 2018; published online Jul. 6, 2018.

1 Introduction

Thousands of exoplanets have been discovered to date and many more will be detected by future missions. The focus of exoplanet studies is shifting toward understanding the statistical properties of exoplanets as a population and detailed characterization for scientifically compelling nearby systems. One of the primary goals of the latter is to study the chemical composition of exoplanet atmospheres and the implications for habitability and life.

Habitability requires a surface temperature that is suitable for life and the existence of liquid water (H_2O). Therefore, H_2O is a high priority species to identity with future telescopes. In addition, biosignature gases, such as oxygen (O_2) and methane (CH_4), are highly indicative of life when coexisting out of thermodynamic equilibrium.[1] Carbon dioxide (CO_2) is the most prominent greenhouse gas and is a key species to identify in habitable exoplanets. The total concentration of CO_2 is expected to differ on a habitable planet based on its position in the habitable zone. A low CO_2 concentration is expected for planets near the inner edge of the habitable zone and a high CO_2 concentration is expected for planets near the outer edge.[2] However, a high concentration of CO_2, together with high stellar UV flux, may produce abiotic O_2.[3–6] In this case, quantifying CO_2, O_2, and other gases will help rule out false-positive scenarios. Future missions to detect and characterize habitable planets will have the ability to identify biosignature gases. However, there are several outstanding technical challenges:

- Bigger aperture: Aperture size of future space missions will be marginally adequate to identify certain biosignature gases. For example, as shown in this paper, it is extremely challenging to detect CH_4 in certain cases.
- Cooler system: Despite much stronger biosignature signals in the near-infrared, it is likely that future large aperture space missions [4 to 6.5 m Habitable Exoplanet Imaging Mission (HabEx) and 8 to 16 Large UV/Optical/IR Surveyor (LUVOIR)] will not have the capability to operate at wavelengths longer than 1.8 μm because of increasing thermal background from the telescope system. To operate beyond 1.8 μm and have reasonably low thermal background, complicated cooling systems would be required, which may drastically increase the cost of the mission.
- Higher spectral resolution bigger aperture: Identifying biosignature gases requires spectroscopic analysis of light from exoplanets. Most proposed dispersing elements for space missions to date have relatively low spectral resolution, e.g., $R \sim 70$ for WFIRST-IFS,[7] which does not take advantage of rich spectral lines of the molecules of interest.
- Better performance of adaptive optics systems: Ground-based extremely large telescopes or giant segment mirror telescopes will face severe challenges in breaking the current starlight suppression floor at 10^{-5} to 10^{-6} level, which is set by adaptive optics system temporal bandwidth to correct for the Earth's atmospheric turbulence.

*Address all correspondence to: Ji Wang, E-mail: ji.wang@caltech.edu

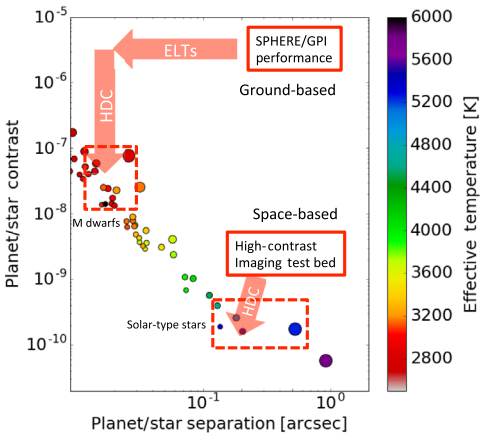

Fig. 1 Planet-star contrast and angular separation for a hypothetical Earth-sized planet in the habitable zone around each star within 5 pc.[8] Each data point is colored by host star effective temperature and the size is scaled with distance. Red solid-lined boxes mark state-of-the-art performance for ground-based direct imaging instruments and test beds for future space-based missions. Red dashed-line boxes indicate the notional objectives for future ground-based missions (i.e., planets around M dwarfs) and for future space missions (i.e., planets around solar-type stars).

Figure 1 summarizes the state-of-the-art performance of direct imaging instruments or testbeds (solid-lined boxes) and the requirements to detect a habitable planet (dashed-lined boxes). For both ground-based and space-based missions, there is a contrast gap between state-of-the-art performance and the planet-star contrast objective.

High-dispersion coronagraphy (HDC) is a recent technical development that is designed to bridge the contrast gap.[9] HDC combines high contrast imaging (HCI), a single-mode fiber injection unit (FIU),[10] and high-resolution spectroscopy (HRS) to filter out stellar light and extract the planet's signal. Specifically, HCI suppresses stellar light and spatially separates the planet from its host star. The FIU filters out stellar noise at the planet location since the electric field of a stellar speckles does not couple to the fundamental mode of a single-mode fiber, whereas up to ~80% of the planet light couples into the fiber. HRS further distinguishes planet signal from stellar signal by its unique spectral features such as absorption lines and radial velocity. Using this three-pronged starlight suppression, HDC can achieve the high sensitivity to study terrestrial planets in the habitable zone.

This paper focuses on the application of HDC on future space telescopes, e.g., HabEx and LUVOIR. The fundamental question we attempt to address here is whether these missions can detect four potential biosignature and habitability marker gases: O_2, CH_4, H_2O, and CO_2, and set mission requirements to achieve this goal. The four molecular species that are chosen have a relatively high concentration in the Earth's atmosphere and are significant signs of life. In addition, these species have been detected in Earthshine and spacecraft observations of our own planet.[11] Detecting other biosignature gases, which have much lower concentrations, is expected to be far more challenging for exoplanets.

The paper is organized as follows. In Sec. 2, we briefly describe the four molecular species we investigate in this paper and the model we use to generate the spectra for our HDC simulations. In Sec. 3, we briefly describe our HDC simulation approach. More details can be found in previous work on HDC.[9,12] Results are given in Sec. 4 followed by summary and conclusion in Sec. 5.

2 Molecular Species of Interest

2.1 *Model Description*

The spectra of Earth-like exoplanets are generated by an atmospheric chemistry and radiative transfer model.[3,13,14] We calculate the molecular abundance as a function of altitude, controlled by photochemical and disequilibrium chemistry processes.[3] The model atmosphere has been compared with terrestrial measurements in the midlatitude and closely resembles the present-day Earth.[3] We calculate the disk-integrated reflected light spectra with an eighth-order Gaussian integration and δ-two-stream approximation. We include the opacities of CO_2, O_2, H_2O, and CH_4 and calculate the planetary flux at a spectral resolution of $R = \lambda/\Delta\lambda = 500{,}000$, which is high enough to resolve individual spectral lines of the aforementioned species over $\lambda = 0.5$ to 5 μm.

It is well known that Earth's disk-averaged spectrum cannot be reproduced by a single surface type or cloud deck.[15–17] Rather, it requires a combination of a cloud-free surface that is poorly reflective (i.e., the ocean), a highly reflective low cloud at ~4 km mimicking the cumulus clouds, and a high cloud at ~12 km mimicking the cirrus clouds.[15] We follow this treatment and assume the three types of surface or cloud. We assign equal weights to the three components to derive a reasonable account for an "Earth-like" planet. While the purpose is to reproduce Earth's spectrum, the resulting spectrum is generally consistent with the Earthshine experiments[15,16] as well as EPOXI measurements.[17]

2.2 *Earth Spectrum by Molecule*

We consider four molecular species in an Earth's atmosphere, CO_2, O_2, H_2O, and CH_4. Their spectra at different spectral resolutions are shown in Fig. 2. Observable line density and line depth decrease as spectral resolution decreases, making detecting certain molecules difficult at low spectral resolutions. Conversely, planet signal is dispersed to more pixels at high spectral resolutions. In such a case, molecule detectability is generally limited by detector noise. Since there are a number of zero- or low-noise detectors that potentially allow us to overcome the detector noise limited case,[18] we assume noiseless detectors in the HDC simulations in this paper.

Planet reflection spectrum is highly dependent on cloud condition. Figure 2 shows four cases: high-cloud, low-cloud, no-cloud, and the average of the three. The high-cloud case (orange) has the highest albedo, but line depth and density are the lowest, because the atmospheric column of absorbing gases above the cloud (~12 km) is the smallest. The effect is more notable for H_2O than for O_2, because the abundance of H_2O drops more than O_2 above the cloud. Consequently, the high-cloud case has the advantage of high reflection but the disadvantage of low spectral information content. In comparison, for the low-cloud case (red), lines are denser and deeper and the albedo is as high as the high-cloud case, so the low-cloud case represents the best case scenario for HDC observations. Lastly, the no-cloud case has the lowest albedo at <0.1, because the cloud-free surface is poorly reflective.

Our averaged spectrum binned down to a low spectral resolution (e.g., $R = 300$) is generally consistent with Earthshine

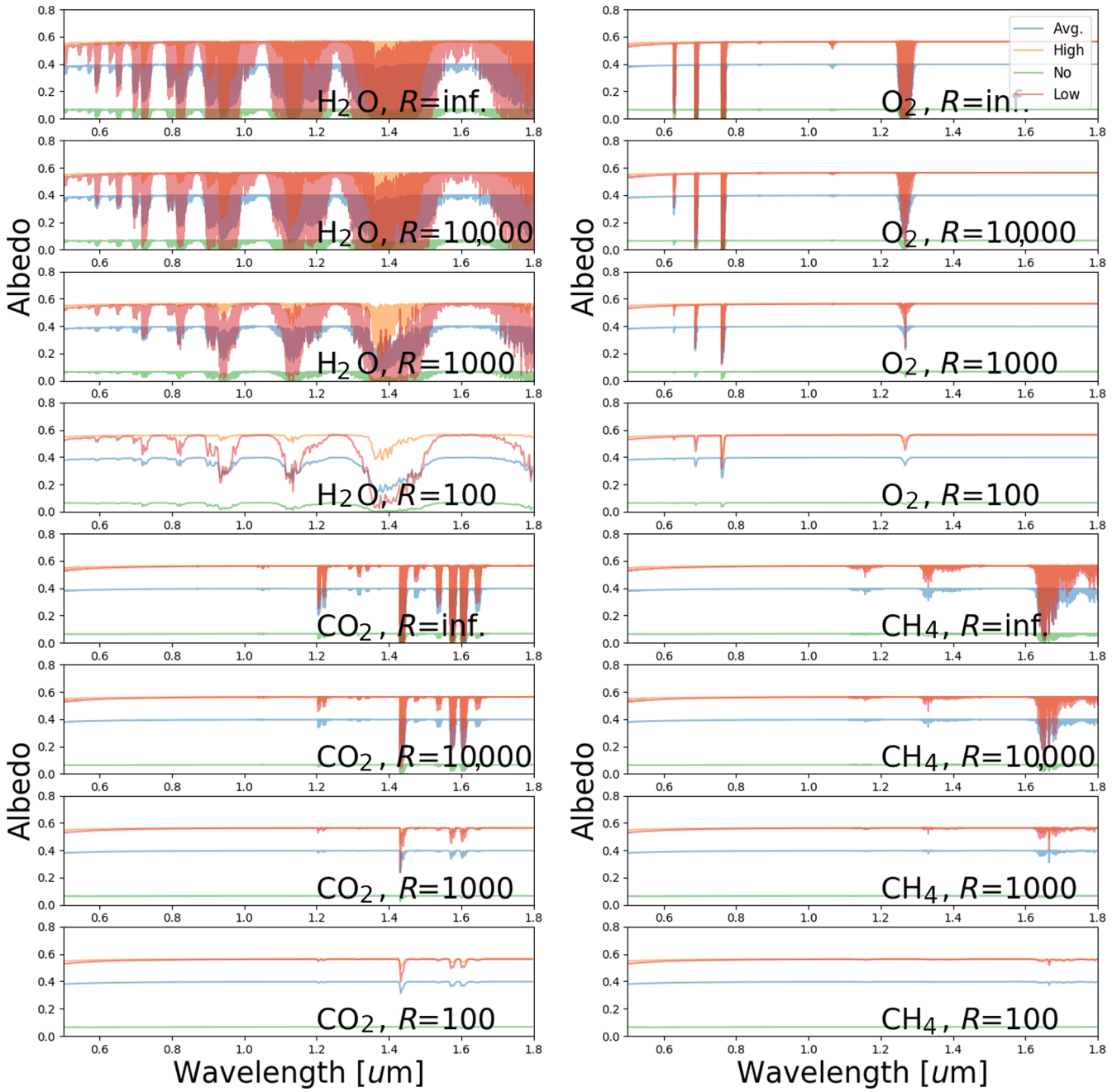

Fig. 2 Albedo spectra for H_2O (top-left), O_2 (top-right), CO_2 (bottom-left), and CH_4 (bottom-right). Colors represent cases with different cloud conditions. Each panel has four rows to show the influence of spectral resolution on spectral features. Top row is for R > 500,000 followed by R of 10,000, 1000, and 100, respectively.

observations.[15] For example, the water absorption feature at 0.95 μm has an absorption depth of ~50% according to Earthshine observation (see Fig. 6 in Ref. 15), consistent with our averaged spectrum (blue in Fig. 2). In comparison, the low-cloud case alone would have a greater continuum albedo and a deeper absorption.

We, however, recognize that the cloud coverage and heights will not be known *a priori* for any planets to be observed. In order to cover a large parameter space, we consider all three cases for different cloud conditions: the low-cloud case, the high-cloud case, and the no-cloud case. Results for the average-cloud case and any other cases should fall within the results of the three cases, which will be discussed in subsequent sections.

Figure 2 also emphasizes the need of going beyond 1 μm to detect biosignature gases. There are no strong lines of CH_4 and CO_2 below 1 μm. Detecting these two molecules is difficult at optical wavelengths. Even for molecules with strong lines below 1 μm, going beyond this wavelength would allow many more strong lines to be measured, thus increasing the detectability. We limit our HDC simulations below 1.8 μm, beyond which a cryogenic space mission would be required.

3 Simulations of HDC Observations

3.1 *Methodology*

In this section, we briefly describe the procedure to simulate HDC observations and conduct data reduction. For more details in HDC simulations, refer to Refs. 9 and 12.

The planet and stellar spectra are convolved with a kernel that corresponds to a certain spectral resolution. The stellar signal is reduced by a factor that we refer to as the starlight suppression level. The starlight suppression includes the suppression from the coronagraph, wavefront control, and additional nulling boost provided by the use of a single-mode fiber.[10]

Poisson noise is added to account for photon noise. In addition, noises incurred in data reduction are included, e.g., errors associated with removing stellar light measured by additional fibers in speckle field. One particularly important noise source, speckle chromatic noise, is also taken into account. This noise arises from wavefront control at high starlight suppression levels and prevents us from detecting biosignature gases at low spectral resolutions.[9]

We briefly discuss here how the speckle chromatic noise confuses biosignature detection at low spectral resolutions and our strategy to remove the confusion. We refer readers to Sec. 6.4 in Ref. 9 for more details. The speckle chromatic noise arises due to wavefront control at deep starlight suppression ($< \sim 10^{-7}$). Because wavefront control is normally optimized at a certain wavelength, starlight suppression is shallower at wavelengths that deviate from the optimal wavelength. As a result, speckle would have a parabolic spectral feature that sometimes mimics an absorption band of a molecule species. We name this speckle behavior at deep starlight suppression levels as the speckle chromatic noise. The speckle chromatic noise may be difficult to distinguish from absorption features of potential biosignatures, and this noise source therefore represents a potential false-positive biosignature absorption signal.

At moderately high spectral resolutions, the speckle chromatic noise is no longer a concern because simulation has shown that the noise only has low-frequency spectral features. Therefore, our strategy of removing the speckle chromatic noise is straightforward. We apply a high-pass filter to those simulated observed spectra to remove spectral features with frequencies that correspond to $R < 100$, where R is spectral resolution. In this procedure, both the speckle chromatic noise and the absorption features are removed. Our HDC simulations are no longer sensitive to spectral features with $R < 100$. However, the simulations are free of the influence of the speckle chromatic noise. This makes direct comparison of our technique incompatible with other works at low resolutions ($R < 100$) that do not use a high-pass filter to mitigate the speckle chromatic noise.

The processed spectrum is then cross-correlated with a template spectrum for the molecular species of interest and at the same spectral resolution as the observation. We note that the processed spectrum contains absorption features of all molecule species and have noise appropriately incorporated and thus represents a realistic case for HDC observations. The resulting cross-correlation function (CCF) is used for biosignature detection and to access the relative abundance of different molecules that are present in planet's atmosphere. The key parameters used in HDC simulations are given in Table 1.

3.2 *Detection Definition*

Each HDC simulation results in a CCF. We repeat the HDC simulation 100 times for each combination of spectral resolution and starlight suppression level. We define significance of detection in the following way. The maximum CCF value within one spectral resolution element to the planet radial velocity is recorded for each run. After 100 runs, the distribution of maximum CCF values is obtained. We then calculate 16 and 84 percentiles, half of the difference between the two values corresponds to $1-\sigma$ of the distribution. This way of defining $1-\sigma$ is robust against outliers. The maximum CCF value divided by $1-\sigma$ gives detection significance. The median of detection significance values for 100 runs is recorded.

4 Results

In this section, we summarize the requirements for detecting certain molecular species in terms of exposure time, spectral resolution, and starlight suppression level. Listed in order of decreasing difficulty, the molecules of interest are: CH_4, CO_2, O_2, and H_2O. The order of O_2 and H_2O may switch depending on spectral resolution and starlight suppression level. Results in this section will provide the baseline requirements for the three cases with different cloud conditions.

4.1 *Requirements for HabEx*

4.1.1 *No-cloud case*

The no-cloud case has the lowest albedo (Fig. 2) and thus represents the worst case scenario. CH_4 cannot be detected even

Table 1 Inputs for HDC simulations for a Sun–Earth system.

Telescope/instrument		Star		Planet	
Telescope aperture	4 or 12 m	T_{eff}	5800 K	Contrast	6×10^{-11}
End-to-end throughput	10%	$\log(g)$	4.5	Planet radius	$1.0R_{\oplus}$
Spectral resolution	Varied	$V \sin i$	2.7 km/s	$V \sin i$	0.5 km/s
Exposure time	Varied	Orbital inclination	50 deg	Orbital phase	0.25
Wavelength	0.5 to 1.8 μm	Radial velocity	0.0 km/s	Radial velocity	20.4 km/s
Detector noise	0	Distance	5 pc	Semimajor axis	1 AU

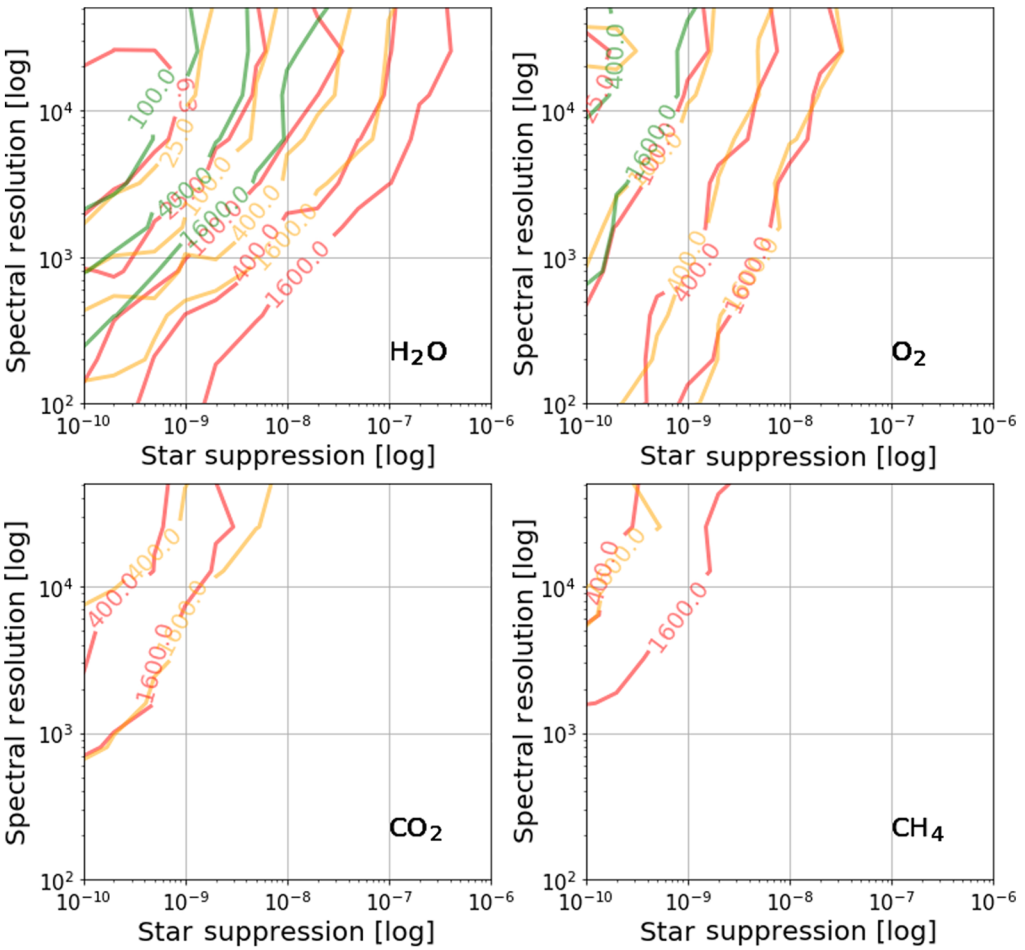

Fig. 3 Exposure time contours (in hours) for 5 – σ detection. Adjacent contours differ by a factor of 4 in exposure time. The simulation is for HabEx and assumes three cases with different cloud conditions: the no-cloud case (green), the high-cloud case (orange), and the low-cloud case (red).

with an exposure time of 1600 h (as shown in green contours in Fig. 3). Because of the low albedo, photon count is extremely low for the 4-m aperture of HabEx, there is on average 0.4 photon per pixel at the highest spectral resolution that we consider ($R = 51{,}200$) for a 100-h integration time. In addition, CH_4 lines are intrinsically rare and shallow at wavelengths shorter than 1.8 μm (see Fig. 2).

Detection of CO_2 is not possible even with an exposure time of 1600 h because of the same reason as the CH_4 case for an albedo <0.1.

The minimum spectral resolution for O_2 detection is at $R = 700$ and $R = 9000$ for 1600- and 400-h exposure time and a starlight suppression level of 1×10^{-10}.

High spectral resolutions are necessary to relax the requirement for starlight suppression for O_2 detection. For example, at $R = 25,600$, starlight suppression can be relaxed to 2×10^{-10} and 1×10^{-9} for 400- and 1600-h exposure time.

The minimum spectral resolution for H_2O detection is at $R \sim 240$ and $R \sim 800$ for 1600- and 400-h exposure time and a starlight suppression level of 1×10^{-10}. Starlight suppression can be relaxed to a few times 10^{-8} at $R = 51{,}200$ for an exposure time of 1600 h. In a comparison to the O_2 case, higher spectral resolutions help more for the H_2O case because of the abundance of water lines across the whole wavelength range.

4.1.2 *High-cloud case*

The high-cloud case has a higher albedo but line depth is much shallower than the no-cloud case. However, the high albedo outweighs the shallow line depth, making it possible to detect all four gases.

The minimum spectral resolution for CH_4 detection is at $R = 5000$ for a 1600-h exposure time and a starlight suppression level of 1×10^{-10}. It has been noted that a higher spectral resolution would help to increase detectability. However, even at $R = 256{,}000$ and 1×10^{-10} starlight suppression, the minimum exposure time is 850 h.

CO_2 can be detected for two exposure times that we consider, 400 and 1600 h, for which the minimum spectral resolution is $R = 8000$ and $R = 700$ at 1×10^{-10} starlight suppression, respectively. At $R = 51{,}200$, the starlight suppression requirement can be relaxed to 5×10^{-9} and 1×10^{-9} for 1600- and 400-h exposure times.

The requirement for O_2 detection is less stringent than CO_2 detection. Spectral resolution higher than 100 will suffice for starlight suppression levels deeper than 2×10^{-10} and 1×10^{-9} for exposure time of 400 and 1600 h. The requirement for starlight suppression is further relaxed toward higher spectral resolutions with increasing exposure time (see orange contours in Fig. 3).

Because the speckle chromatic noise[9] is considered in our simulation, any low-frequency spectral features are removed because of a high-pass filter that we have applied in the data reduction procedure. As a result, no molecules can be detected at a spectral resolution lower than $R = 100$.

The minimum exposure time for H_2O detection is 12.7 h at $R = 25{,}600$ and $C = 1 \times 10^{-10}$, where C denotes starlight suppression level. The requirement for starlight suppression can be relaxed by three orders of magnitude (compared to planet-star contrast at $\sim 10^{-10}$) at high spectral resolutions ($R > 25{,}600$) and for a long exposure time (i.e., 1600 h). In this regime, the sensitivity boost of high dispersion coronagraphy is fully taken advantage because of sufficient photon flux and high spectral resolution.

4.1.3 *Low-cloud case*

The main difference between the low-cloud case and the high-cloud case is line depth and density (see Fig. 2): spectral information is richer for the low-cloud case, which makes the case more amenable for spectroscopic observation. Red contours in Fig. 3 shows $5-\sigma$ detection significance contour. Notably, the $5-\sigma$ extends to lower spectral resolutions and shallower starlight suppression levels for H_2O and CH_4. Consequently, detection of these two molecule species is easier than the high-cloud case. This can be explained as follows: atmospheric column density for H_2O and CH_4 drops more than CO_2 and O_2, so a high cloud affects H_2O and CH_4 detectability more than CO_2 and O_2.

For CH_4, minimum exposure time is 300 h at $R = 51{,}200$ and $C = 1 \times 10^{-10}$. For longer exposure times, the requirement for both spectral resolution and starlight suppression can be relaxed. For example, the minimum spectral resolution is at $R = 1400$ and $R = 5000$ at $C = 1 \times 10^{-10}$ for exposure time of 1600 and 400 h. At a spectral resolution of 51,200, starlight suppression can be relaxed to 3×10^{-10} and 2×10^{-9} for exposure time of 400 and 1600 h.

Detection of CH_4 in different cloud conditions exemplifies the influence of planetary spectrum on detection. The variety of possible planetary spectra may be the major uncertainty in estimating the minimum requirements for future space missions in search for biosignatures. We show here the influence of cloud condition. There are other uncertainties that may affect the mission sensitivity to biosignatures, for instance, the time evolution of Earth atmosphere. CH_4 concentration was much higher in Archean Earth atmosphere.[19] Therefore, it is much easier to search for CH_4 for an Archean Earth.

The minimum exposure time for CO_2 detection is 150 h at $R = 51{,}200$ and $C = 1 \times 10^{-10}$. The minimum spectral resolutions are $R = 700$ and $R = 2200$ for exposure time of 1600 and 400 h at a starlight suppression level of 1×10^{-10}. At the highest

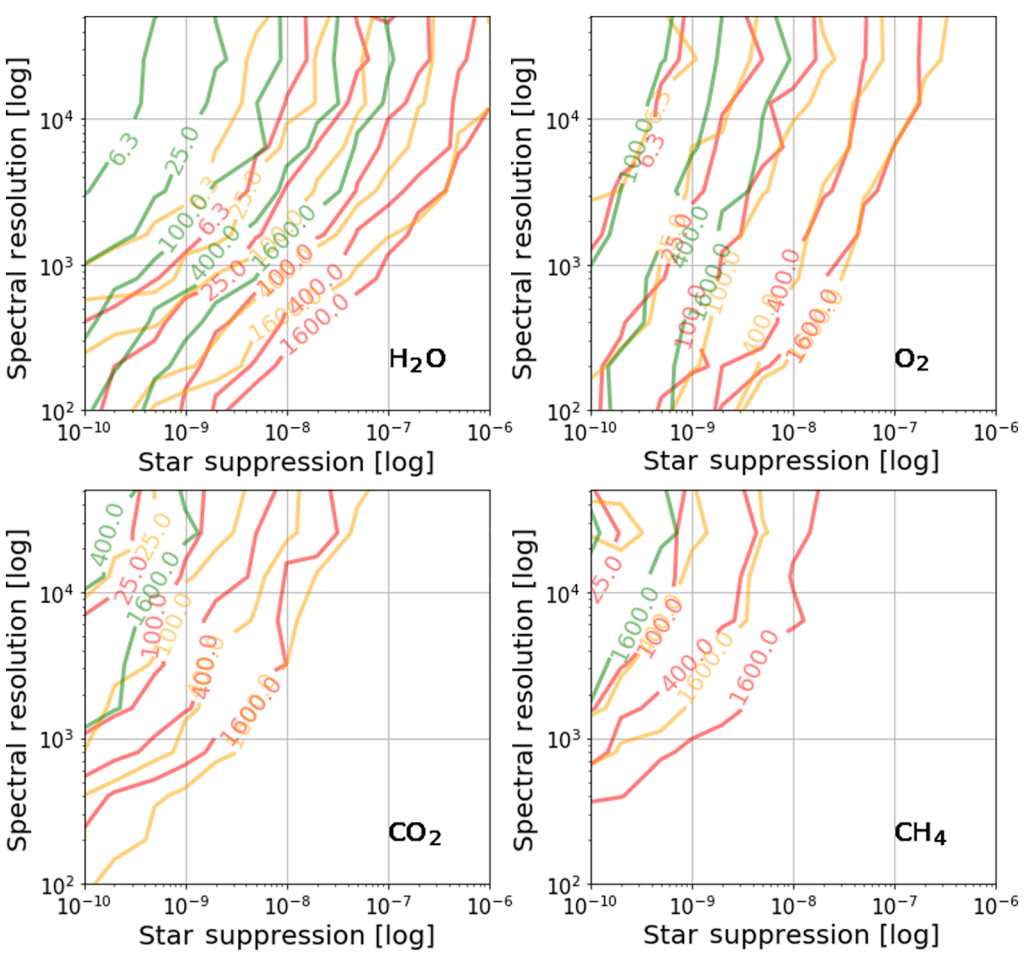

Fig. 4 Exposure time contours (in hours) for $5-\sigma$ detection. Adjacent contours differ by a factor of 4 in exposure time. The simulation is for LUVOIR and assumes three cases with different cloud conditions: the no-cloud case (green), the high-cloud case (orange), and the low-cloud case (red).

spectral resolution, we consider ($R = 51{,}200$) the minimum starlight suppression requirements are 7×10^{-10} and 2×10^{-9} for exposure time of 400 and 1600 h.

The requirement for O_2 detection is similar to that for the high-cloud case.

The minimum exposure time for H_2O detection is 5 h at $R = 12{,}800$ and $C = 1 \times 10^{-10}$. The requirement for starlight suppression can be relaxed by three orders of magnitude (compared to planet-star contrast at $\sim 10^{-10}$) at high spectral resolutions ($R > 25{,}600$) and for long exposure times (>400 h).

4.2 *Requirements for LUVOIR*

4.2.1 *No-cloud case*

Green contours in Fig. 4 show $5-\sigma$ detection contours at different exposure times for biosignatures for the LUVOIR no-cloud case. With a bigger aperture and thus higher photon flux, detection significance contours extend to lower spectral resolutions and shallower starlight suppression levels. Notably, the starlight suppression requirements are relaxed to $\sim 10^{-8}$ and 2×10^{-9} for H_2O and O_2 for an exposure time of 100 h. We expect 100 h as a reasonable exposure time for LUVOIR because it is a general purposed mission. CO_2 and CH_4 are not detectable given the 100-h exposure time. The minimum exposure time for CO_2 and CH_4 detection is 183 and 354 h at $R = 25{,}600$ and $C = 1 \times 10^{-10}$. At the same combination of spectral resolution and starlight suppression level, the minimum exposure time for H_2O and O_2 detection is 5.0 and 25.0 h.

4.2.2 *Low-cloud case*

Red contours in Fig. 4 show $5-\sigma$ detection contours at different exposure times for biosignatures for the LUVOIR low-cloud case. This represents the best case scenario for biosignature search among all that we have considered in this paper. With an exposure time that shorter than 25 h, all biosignatures can be detected at $R = 51{,}200$ and $C = 1 \times 10^{-10}$. However, we must point out that the minimum exposure time is very sensitive to what type of cloud a planet may have. The minimum exposure time usually varies by a large factor. For example, the minimum exposure time for CH_4 detection differs by a factor of more than 10 between the no-cloud case (354 h) and the low-cloud case (24 h).

4.2.3 *High-cloud case*

Orange contours in Fig. 4 shows $5-\sigma$ detection contours at different exposure times for biosignatures for the LUVOIR high-cloud case. For, H_2O and CH_4, the high-cloud contours recede toward higher spectral resolutions and deeper starlight suppression (i.e., upper-left corner of the parameter space in Fig. 4) when compared to the low-cloud case, indicating lower detectability of these two species in the high-cloud case. The high-cloud contours for O_2 are comparable between the low-cloud case and the high-cloud case, which is consistent with the HabEx result. The high-cloud contours for CO_2 indicate a higher detectability than the low-cloud case. However, we will show in Sec. 5.1 that the detectability is in fact comparable within uncertainties in exposure time calculation.

5 Summary and Conclusion

We study the detectability of four molecular species as biosignature or habitability indicators: CH_4, CO_2, O_2, and H_2O. We conduct HDC simulations to set the minimum requirements of exposure time, spectral resolution, and starlight suppression for the detection of these biosignatures. Major findings are summarized in Figs. 3 and 4. The implications are discussed in details in Sec. 4. The results provide a baseline for mission design in order to search for biosignature gases and study the habitability of exoplanets.

The results of this paper are based on HDC simulations that focus on performance at high spectral resolutions. While the simulations are compatible with low-resolution results, the cross-correlation may not be the best possible way to detect planets or molecules. A more straightforward way is to conduct a conventional ADI/SDI sequence, detecting the planet, obtaining a low-resolution spectrum, and inferring the molecular presence by measuring the absorption band depth. However, we provide two arguments for using the cross-correlation technique at low spectral resolutions. First, this ensures consistency in comparing performance over a broad range of spectral resolutions. Second, speckle chromatic noise may hinder molecule detection at low spectral resolutions with conventional method, the treatment in our HDC simulation ensures the effect of the speckle chromatic noise is properly modeled and removed.

5.1 *Comparison to Previous Results*

One major difference between this work and previous works on observing Earth-like planet using low-resolution spectroscopy:[20] we consider speckle chromatic noise, which is a significant noise source at low spectral resolution (e.g., $R < 100$).

Another difference is the definition of detection significance. In this work, we adopt the local variation of CCF peaks rather than the variation estimated from other parts of CCF. In previous works, the variation was estimated using the fluctuation of first quarter and/or the fourth quarter of CCF. In principle, there should be no significant difference. However, using the local variation is more representative of CCF variation around CCF peak.

We compare our results to previous HDC simulations for HabEx and LUVOIR.[9,21] Using the same input planet spectrum, i.e., the average of the no-cloud case and the low-cloud case, we compare the results for HabEx 400-h exposure and LUVOIR 100-h exposure (Fig. 5) to Figs. 20 and 15 in Ref. 9 to quantify the influence of difference definition of detection significance. We find that the contours in these two works track each other well with a maximum horizontal (i.e., starlight suppression level) difference by a factor of 2 at spectral resolution higher than $R \sim 2000$. Part of the difference arises from statistical noise as it is evident that the contours are not smooth. The major difference between results in this paper and Figs. 20 and 15 in Ref. 9 is that we include speckle chromatic noise, which affects results at low spectral resolution significantly. Therefore, it is expected that contours in Fig. 5 deviate from contours in Figs. 20 and 15 in Ref. 9 at lower spectral resolutions.

We also compare our results to Table 2 in Ref. 21 to check the consistency of exposure time calculation for different definitions of detection significance. We can check only one HabEx case for starlight suppression level shallower than 10^{-10} because HDC simulations in this work do not go deeper than 10^{-10}. At $R = 6400$ and $C = 5 \times 10^{-10}$, the exposure time for O_2 and H_2O detection is 162 and 404 h. These values are comparable with values in Table 2 in Ref. 21 within a factor or 1.6. We also compare results for two LUVOIR cases ($R = 6400$ and $R = 25{,}600$

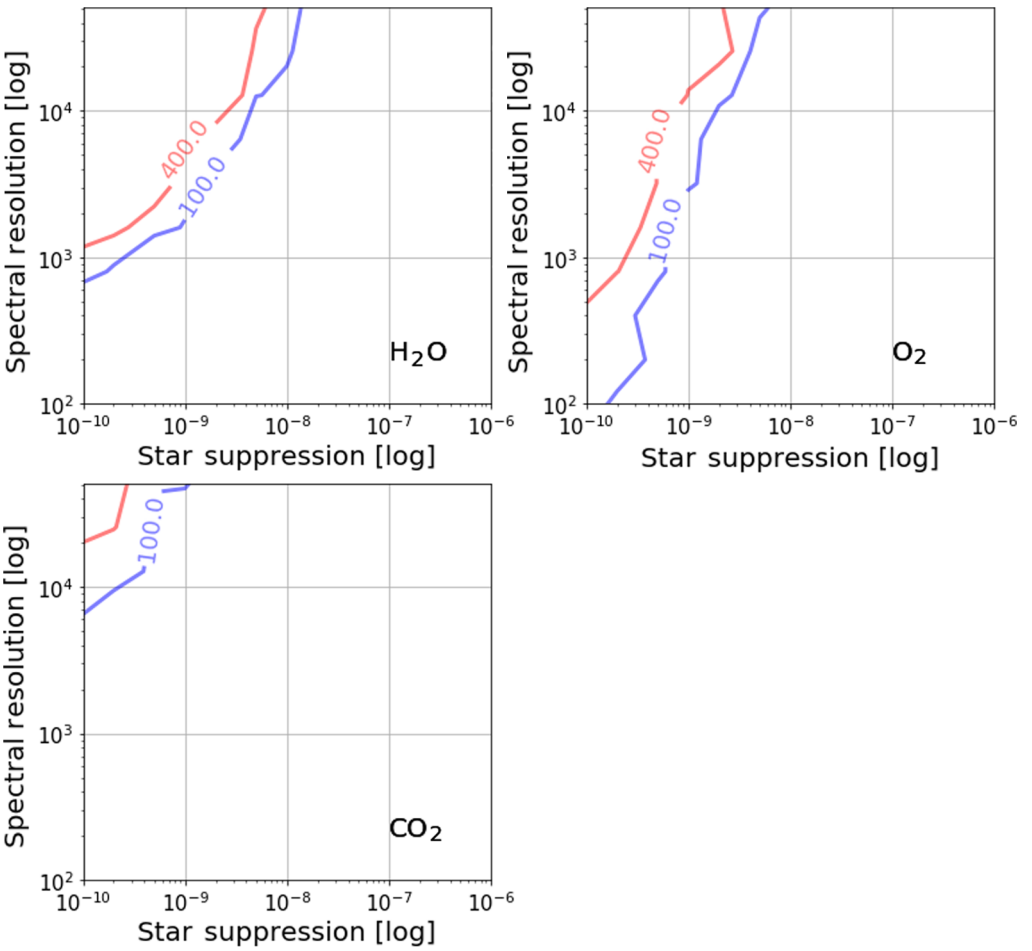

Fig. 5 Exposure time contours (in hours) for $5-\sigma$ detection. Blue contours are for LUVOIR and red contours are for HabEx.

at $C = 1 \times 10^{-9}$). For $R = 6400$ and $C = 1 \times 10^{-9}$, the exposure time for CH_4, CO_2, O_2, and H_2O detection is >1600, 406.2, 72.1, and 25.5 h. Except for CH_4, exposure times for all other species are within a factor of 1.4 when compared to values in Table 2 in Ref. 21. For CH_4, we have a lower limit for exposure time because our simulation stops at 1600 h. For $R = 25{,}600$ and $C = 1 \times 10^{-9}$, the exposure time for CO_2, O_2, and H_2O detection is 196.0, 39.0, and 18.0 h. These values are also within a factor of 2 to values in Ref. 21.

Given the comparison with previous works, we conclude that the uncertainty of exposure time due to definition of detection significance and Poisson statistical noise is at most a factor of 2. This uncertainty is smaller than the uncertainty due to cloud condition, which can change exposure time by a factor of ~10 between the low-cloud case and the no-cloud case. To account for the uncertainty of different definition of detection significance, we advise readers to use an error bar of 0.3 dex (i.e., a factor of 2) when using the minimum exposure time estimated in this paper for a given case of cloud condition.

For the speckle chromatic noise, we use a high-pass filter to remove speckle chromatic noise. As a result, low-frequency spectral features are also removed. This results in a much longer exposure time at low spectral resolution to reach a certain detection significance. For example, the exposure time is 80 h for $R = 100$ and $C = 1 \times 10^{-10}$ for O_2 detection. In comparison, Ref. 20 estimated the exposure time is 200 h for $R = 70$ and $C = 1 \times 10^{-10}$. The difference can be explained as follows. First, the distance of the planet in their calculation was 10 pc. Factoring the difference would reduce the exposure time from 200 to 50 h. Second, our error bar is 0.3 dex, so the actual exposure time can vary from 40 to 160 h depending on the definition of detection significance. Therefore, the two results are consistent within uncertainty.

5.2 *Exozodiacal Flux and Thermal Background*

We consider in our HDC simulation only starlight suppression levels that expected to be achieved by a coronagraphic system. However, the flux from exozodiacal dust may set a floor for the achievable starlight suppression level. This floor is estimated at a few times the planet-star contrast for a 4-m aperture, i.e., $\sim 10^{-10}$.[22,23] LUVOIR designs are less prone to exozodiacal flux because of a smaller point spread function and thus smaller contamination area. This is a result of the larger aperture of LUVOIR.

Another noise source that is not accounted for in our HDC simulation is the thermal background emission from the telescope and instrument. This is not a typical concern at optical wavelengths. However, thermal background quickly becomes a severe issue at longer wavelengths. It is possible to consider a cryogenic system that cools the instrument to minimize thermal background and allows the instrument to operate at longer

wavelengths. For example, mission designs exist that cool the system to 130 K without active cryogenic cooling: Euclid uses a passive cooling radiator system to cool the system to 130 K.[24] To be more realistic, we will incorporate both exozodiacal light emission and thermal noise in future versions of HDC simulation packages.

5.3 *Inner Working Angle in Near Infrared Observation*

While observing in near-infrared wavelengths probes biosignatures, such as CH_4, which is otherwise undetected in optical wavelengths, there are challenges for coronagraphic observations: the inner working angle (in unit of λ/D) decreases due to increasing wavelengths for a given planet-star separation. For example, an Earth–Sun system at 10 pc has an angular separation of $0.1''$. In comparison, 1 λ/D for a 4-m HabEx at 1.7 μm, where CH_4 features are, is $0.087''$. While extremely challenging, new concepts have been proposed to address coronagraphy at sub-λ/D, e.g., the Single-mode Complex Amplitude Refinement (SCAR) coronagraph,[25,26] and the vortex fiber nuller (VFN). Moreover, given the long exposure time that is required to search for biosignatures for a 5-pc system, observing nearby systems much closer than 10 pc will not only keep the exposure time tractable but also alleviate the inner working angle problem

Acknowledgments

We would like to thank Rowan Swain for proofreading the manuscript. We thank anonymous referees for their comments and suggestions that greatly improve the paper.

References

1. D. J. Des Marais et al., "Remote sensing of planetary properties and biosignatures on extrasolar terrestrial planets," *Astrobiology* **2**, 153–181 (2002).
2. R. K. Kopparapu et al., "Habitable zones around main-sequence stars: new estimates," *Astrophys. J.* **765**, 131 (2013).
3. R. Hu, S. Seager, and W. Bains, "Photochemistry in terrestrial exoplanet atmospheres. I. Photochemistry model and benchmark cases," *Astrophys. J.* **761**, 166 (2012).
4. S. D. Domagal-Goldman et al., "Abiotic ozone and oxygen in atmospheres similar to prebiotic earth," *Astrophys. J.* **792**, 90 (2014).
5. F. Tian et al., "High stellar FUV/NUV ratio and oxygen contents in the atmospheres of potentially habitable planets," *Earth Planet. Sci. Lett.* **385**, 22–27 (2014).
6. C. E. Harman et al., "Abiotic O_2 levels on planets around F, G, K, and M stars: possible false positives for life?," *Astrophys. J.* **812**, 137 (2015).
7. M. W. McElwain et al., "PISCES: an integral field spectrograph technology demonstration for the WFIRST coronagraph," *Proc. SPIE* **9904**, 99041A (2016).
8. Oliver Guyon, "Habitable Zone Planets for ELTs," https://www.naoj.org/staff/guyon/.
9. J. Wang et al., "Observing exoplanets with high dispersion coronagraphy. I. The scientific potential of current and next-generation large ground and space telescopes," *Astron. J.* **153**, 183 (2017).
10. D. Mawet et al., "Observing exoplanets with high-dispersion coronagraphy. II. Demonstration of an active single-mode fiber injection unit," *Astrophys. J.* **838**, 92 (2017).
11. S. Seager, W. Bains, and J. J. Petkowski, "Toward a list of molecules as potential biosignature gases for the search for life on exoplanets and applications to terrestrial biochemistry," *Astrobiology* **16**, 465–485 (2016).
12. J. Wang et al., "High-contrast imaging and high-resolution spectroscopy observation of exoplanets," *Proc. SPIE* **9911**, 99112T (2016).
13. R. Hu, S. Seager, and W. Bains, "Photochemistry in terrestrial exoplanet atmospheres. II. H_2S and SO_2 photochemistry in anoxic atmospheres," *Astrophys. J.* **769**, 6 (2013).
14. R. Hu and S. Seager, "Photochemistry in terrestrial exoplanet atmospheres. III. Photochemistry and thermochemistry in thick atmospheres on super earths and mini Neptunes," *Astrophys. J.* **784**, 63 (2014).
15. M. C. Turnbull et al., "Spectrum of a habitable world: earthshine in the near-infrared," *Astrophys. J.* **644**, 551–559 (2006).
16. G. Tinetti et al., "Detectability of planetary characteristics in disk-averaged spectra. I: the earth model," *Astrobiology* **6**(1), 34–47 (2006).
17. T. D. Robinson et al., "Earth as an extrasolar planet: earth model validation using EPOXI earth observations," *Astrobiology* **11**(5), 393–408 (2011).
18. B. J. Rauscher et al., "Detectors and cooling technology for direct spectroscopic biosignature characterization," *J. Astron. Telesc. Instrum. Syst.* **2**, 041212 (2016).
19. S. Rugheimer and L. Kaltenegger, "Spectra of earth-like planets through geological evolution around FGKM stars," *Astrophys. J.* **854**(1), 19 (2018).
20. T. D. Robinson, K. R. Stapelfeldt, and M. S. Marley, "Characterizing rocky and gaseous exoplanets with 2 m class space-based coronagraphs," *Publ. Astron. Soc. Pac.* **128**, 025003 (2016).
21. J. Wang et al., "Baseline requirements for detecting biosignatures with the HabEx and LUVOIR mission concepts," *Proc. SPIE* **10400**, 104000Z (2017).
22. A. Roberge et al., "The exozodiacal dust problem for direct observations of exo-earths," *Publ. Astron. Soc. Pac.* **124**, 799–808 (2012).
23. C. C. Stark et al., "Maximizing the exoearth candidate yield from a future direct imaging mission," *Astrophys. J.* **795**, 122 (2014).
24. G. D. Racca et al., "The Euclid mission design," *Proc. SPIE* **9904**, 99040O (2016).
25. E. H. Por and S. Y. Haffert, "The single-mode complex amplitude refinement (SCAR) coronagraph: I. Concept, theory and design," arXiv:1803.10691 (2018).
26. S. Y. Haffert et al., "The single-mode complex amplitude refinement (SCAR) coronagraph: II. Lab verification, and toward the characterization of proxima b," arXiv: 1803.10693 (2018).

Ji Wang is currently a postdoc at Caltech. He attended the University of Science and Technology of China (USTC) for his undergraduate study. He obtained his PhD from the University of Florida and worked as a postdoc at Yale University before moving to Caltech.

Biographies for the other authors are not available.